JOURNAL OF AIRCRAFT
Vol. 45, No. 5, September–October 2008

Computational Prediction of Nose-Down Control for F/A-18E at High Alpha

Bradford E. Green*
Naval Air Systems Command, Patuxent River, Maryland 20670

DOI: 10.2514/1.34562

Computational fluid dynamics was used to predict the longitudinal stability and control characteristics of the preproduction F/A-18E Super Hornet configuration with neutral and full nose-down control at high angle of attack, subsonic conditions. Such data contribute to an analysis of the ability of the pilot to recover from extreme angles of attack and are usually obtained and extrapolated from wind-tunnel tests. The current computational study was intended to be an exploratory study of the usefulness of computational fluid dynamics to aid the designer and analysts in predictions of flight behavior. The calculations were made for Mach 0.082 at a Reynolds number of 1.15×10^6 based on mean aerodynamic chord at angles of attack between 0 and 60 deg. The F/A-18E was modeled with 34-deg leading-edge flaps, 4-deg trailing-edge flaps, 0-deg aileron deflection, a rudder deflection of 30 deg, a spoiler deflection of 60 deg, and horizontal-tail deflections of 0 and 20 deg. The flow conditions and configuration corresponded to those used in tests of a 15%-scale F/A-18E wind-tunnel model tested at the 30- by 60-ft full-scale wind tunnel at the NASA Langley Research Center in Hampton, Virginia. The flow solver used during this project was USM3D, which was developed by the NASA Langley Research Center. The forces and moments predicted by USM3D compared well to the wind-tunnel data for angles of attack between 0 and 40 deg. For angles of attack from 40 to 60 deg, however, the results from USM3D differed from the wind-tunnel data. These differences are attributed to the unsteady nature of the flow and turbulence effects not adequately captured by the computations.

Nomenclature

C_A = axial-force coefficient
C_D = drag coefficient
C_L = lift coefficient
C_m = pitching-moment coefficient
C_N = normal-force coefficient
R = nondimensional L-2 norm of the mean-flow residual
Re_c = Reynolds number based on mean aerodynamic chord
α = angle of attack, deg
δ_s = horizontal-tail deflection angle, deg

I. Introduction

THE analysis of stability and control (S&C) characteristics of aircraft involves the analysis of behavior at and beyond the edge of the flight envelope. At these conditions, aerodynamic characteristics are difficult to predict due to massive flow separation, effects of aircraft dynamic motions, and time-dependent phenomena. Traditionally, wind tunnels have been used by the S&C community to analyze the characteristics of aircraft in this difficult flow regime. Wind tunnels, however, have limitations (Reynolds number, for example) and sometimes cannot accurately predict the aerodynamic characteristics of the aircraft. Whereas computational fluid dynamics (CFD) could theoretically be used to model aircraft aerodynamics at flight conditions at and beyond the edge of the envelope, CFD has not yet been fully calibrated and proven for these conditions. This computational effort represents an initial exploratory investigation into using CFD for predicting the S&C characteristics of aircraft.

Because of the inherent difficulty in accurately predicting the S&C characteristics of the aircraft at the edge of the envelope, nearly every advanced aircraft program has been surprised by unpredicted, undesirable aerodynamic phenomena [1]. Eliminating these undesirable characteristics is both costly and time consuming because of the amount of wind-tunnel testing and "cut and try" flight testing involved. As a result, it is desirable to find and fix problems early in a program. Whereas CFD could be used in conjunction with wind-tunnel tests to find potential problems, S&C engineers in general lack confidence in CFD due to the lack of applications and calibrations of the codes. CFD has been used with success to predict the aerodynamic performance of aircraft and for flow diagnostics, but CFD has not been widely used for force and moment calculations for S&C. This "gap" between the traditional uses of CFD and the needs of the S&C community has made it difficult for CFD users to earn the support of the S&C engineers.

As a result of the gap between CFD users and the S&C community, the National Aeronautics and Space Administration (NASA), with participation from the Department of Defense and industry, started the Computational Methods for Stability and Control (COMSAC) program in 2004. The COMSAC program was formed to focus CFD tools to applications in S&C and to improve communications between CFD and S&C specialists. In September 2003 in Hampton, Virginia, the COMSAC program brought together over 100 CFD experts and S&C engineers from government and industry to share their present and future needs.

In recent years, several researchers have been applying CFD to complex S&C problems in an effort to show the S&C community that CFD can be accurate and fast. Many of these applications have required code development to improve the speed and accuracy of the calculations. Cummings et al. [2] presents a good overview of the difficulties in predicting flows at high angles of attack. Cummings et al. list six issues that are important when looking at high angle-of-attack flows. These issues include the complexity of the governing equations, turbulence modeling, transition modeling, algorithm symmetry, grid generation and density, and numerical dissipation. Cummings et al. also indicate that time-accurate solutions using detached-eddy simulation (DES) [3] is often required to obtain good correlations with data for high angle-of-attack flows.

Forsythe et al. [4] used CFD to predict the massively separated flow around the F-15E at $\alpha = 65$ deg. The aircraft was clean, without any stores or control deflections. The calculations were performed using the Spalart–Allmaras (SA) turbulence model in

Presented as Paper 6724 at the AIAA Atmospheric Flight Mechanics Conference, Hilton Head, SC, 20–23 August 2007; received 12 September 2007; revision received 24 March 2008; accepted for publication 25 March 2008.

*Aerospace Engineer, Advanced Aerodynamics Branch, Building 2187, Unit 5, Suite 1320-B, 48110 Shaw Road. Senior Member AIAA.

steady-state mode and the DES method with SA in time-accurate mode. Forsythe et al. found that the lift, drag, and pitching moment could be predicted within 10% of the data using the steady-state calculation, although the DES results agreed more favorably with the data. Forsythe et al. noted that the time-accurate calculations were seven times more expensive than the steady-state calculations on the same grid. Forsythe et al. [5], building on the results from [4], used CFD to evaluate the F-15E in spin without any stores or control deflections.

The goal of the current project was to assess the ability of CFD to predict the longitudinal S&C characteristics of the preproduction F/A-18E Super Hornet configuration with neutral and full nose-down control at high-angle-of-attack, subsonic conditions. Such data contribute to an analysis of the ability of the pilot to recover from extreme angles of attack. These calculations were conducted on the F/A-18E with leading-edge flaps, trailing-edge flaps, rudder, horizontal tail, and spoiler deflected. It is believed that these are the first calculations on the F/A-18E with full nose-down control and possibly the first CFD calculations on any military aircraft with full nose-down control.

This effort was meant to be an initial exploratory investigation into calculating the S&C characteristics for the F/A-18E with full nose-down control. Because S&C engineers often complain about the length of time required for CFD calculations, the majority of these calculations were performed in steady-state mode. It is well understood that high-angle-of-attack flows are often unsteady. However, based on the results of Forsythe et al. [4], it is possible to obtain reasonable results at high angles of attack with steady-state calculations. Although not part of the original project plan, a few calculations were performed at high angles of attack using a time-accurate approach to show the benefits of such calculations.

The calculations for this study were made for Mach 0.082 at a Reynolds number of 1.15×10^6 based on mean aerodynamic chord at angles of attack between 0 and 60 deg using the USM3D flow solver. USM3D is a Navier–Stokes flow solver for unstructured tetrahedral grids. The F/A-18E was modeled with 34-deg leading-edge flaps, 4-deg trailing-edge flaps, 0-deg aileron deflection, rudder deflections of 30 deg, a spoiler deflection of 60 deg, and horizontal-tail deflections of 0 and 20 deg. The flow conditions and configuration corresponded to those used in tests of a 15%-scale F/A-18E wind-tunnel model tested at the 30- by 60-ft full-scale wind tunnel at NASA Langley Research Center in Hampton, Virginia.

The first step during this study was to perform a grid-resolution study. Grid sizes of 9.9 and 18.0 million cells were used to predict the forces and moments on the aircraft for angles of attack between 5 and 35 deg. Based on these results, it was determined that the 9.9 million cell grid was capable of predicting the forces and moments on this configuration within a sufficient accuracy. As a result of the grid-resolution study, grids with 9.9 million cells were used to predict the forces and moments on the configuration with horizontal-tail deflections of 0 and 20 deg at angles of attack between 0 and 60 deg. The CFD calculations were performed "blind," without prior knowledge of the wind-tunnel data. The forces and moments of these configurations, as well as the pitching-moment increment between the two configurations, were then compared with the existing wind-tunnel data. Whereas the majority of the calculations for this study were conducted in steady-state mode, time-accurate calculations were conducted at a single high-angle-of-attack condition to show the benefits of time-accurate calculations.

The work presented herein represents the second phase of a larger project. In the first phase of the project, CFD was used to predict the static longitudinal and lateral/directional stability and control characteristics of the preproduction F/A-18E at two transonic Mach numbers. The correlation of CFD with the wind-tunnel data was generally very good. More work is required, however, to analyze differences apparently due to the effects of unsteadiness near wing stall. The agreement between the CFD results and the wind-tunnel data for the longitudinal stability and control characteristics was good, although the agreement near wing stall was poor. The general character of the longitudinal control effectiveness was predicted reasonably well by the code. For the most part, CFD did a good job of predicting the lateral/directional stability and control characteristics of the aircraft at the transonic conditions. At wing stall, large differences existed between results from two wind tunnels as well as CFD. Above wing stall at Mach 0.9, the CFD results were dependent upon the initial condition of the calculation because of the unsteady nature of the flow. Redoing the calculations with different initial conditions resulted in good agreement between wind tunnel and CFD. The results of this work are presented in their entirety in [6].

The work on this project came as a result of the COMSAC initiative described previously. Funding for this project came from the Common High Performance Computing Software Support Initiative (CHSSI). This project was dedicated to making improvements to CFD codes that would improve their ability to quickly and accurately predict the S&C characteristics of complex aircraft configurations at challenging flight conditions. This project, named Integrated Simulation of Air Vehicle Performance, Stability, and Control for Test and Evaluation, was within the Collaborative Simulation and Testing (CST) integrated portfolio. This project was composed of engineers from the Naval Air Systems Command, NASA Langley Research Center, the Air Force Research Laboratory, and numerous contractors and consultants.

In the next section, a description of the wind-tunnel test used for validation of the CFD results will be discussed. In the following section, the grid generator and flow solver used during this study are discussed. A description of the geometry and grids is included in the subsequent section. In the next section, the computer requirements and solution convergence are discussed, followed by results of a grid-refinement study. CFD predictions of longitudinal stability and control characteristics are then compared with the wind-tunnel data in the next section. The impacts of turbulence model and grid density are discussed in the following section. The results of some time-accurate calculations with several different turbulence models are then presented. Finally, some conclusions of the study are offered.

II. Description of Wind-Tunnel Test Used for Computational Fluid Dynamics Validation

A. Summary

The wind-tunnel test that was used to validate the F/A-18E CFD calculations that are presented herein was conducted at the Langley Full-Scale Tunnel (LFST) [7], which is located on Langley Air Force Base in Hampton, Virginia. The test was conducted by Bihrle Applied Research (BAR) of Hampton, Virginia. The test was a low-speed aerodynamic force and moment static wind-tunnel test that was conducted on a 15%-scale model of the F/A-18E/F. The primary purpose of the test was to evaluate the effects of the leading-edge extension (LEX) vents on the basic airframe and on the control characteristics of the aircraft. The test was conducted on the T-bar model support located on the centerline of the 30×60 ft test section at a dynamic pressure of 10 psf. Both angle-of-attack and angle-of-sideslip sweeps were conducted. The angle-of-attack range for the test was −4–65 deg. The high angle-of-attack and large-sideslip data were collected to augment the aerodynamic database of the F/A-18E/F aircraft simulation.

B. Model Description

The model that was tested during this entry was the 15%-scale F/A-18E/F low-speed aero model. This model was built by NASA for static, forced oscillation and free-flight testing. The model was used for the previous NASA small model support (SMS) test entries. The model was constructed of fiberglass with a wood and aluminum structure, and incorporated flow-through ducts, adjustable surfaces, and an aft entry sting mounting system, and it could accommodate a six-component balance mounted internally. All main control surfaces (leading-edge and trailing-edge flaps, ailerons, horizontal tails, rudders, LEX spoilers, and LEX vents) were movable and could be set to any deflection within the travel limits for the actual aircraft. External stores, interchangeable cruise and afterburner nozzles, and an E or F canopy were some of the reconfigurable elements of the model.

C. Test Facility

The wind-tunnel test was conducted at the Langley Full-Scale Tunnel [7], which is operated by Old Dominion University, in August 2001. The tunnel is housed in a $434 \times 222 \times 90$ ft building on Langley Air Force Base in Hampton, Virginia. The test section is 30 ft high by 60 ft wide by 56 ft long. The tunnel is a closed-circuit, double-return, open-throat, continuous-flow design that operates at atmospheric pressure. It is powered by 2 four-bladed, 35.5-ft-diam fans, each driven by a 4000-hp electric motor, providing for a maximum speed of approximately 100 mph.

The model was attached to a hydraulically actuated model support that used stings mounted on a T bar spanning the full-scale support system main struts. The actuator generated vertical pitch motion. The entire model support was mounted in the center of a turntable mechanism on the ground board. The rotation of the turntable combined with the pitch motion of the model support system produced the desired angle-of-attack and angle-of-sideslip combinations for the model.

D. Test Conditions

The test was conducted at a dynamic pressure of 10 psf and an airspeed of approximately 92 ft/s. The corresponding Reynolds number was approximately 1.15×10^6 based on the mean aerodynamic chord of the model or about 600,000 per foot. The six-component force and moment data were reduced for a moment reference center located at 25% of the mean aerodynamic chord.

III. Discussion of Grid Generator and Flow Solver

The Tetrahedral Unstructured Software System (TetrUSS) [8] was used to generate and analyze grids of the preproduction F/A-18E during this study. TetrUSS was developed by researchers at the NASA Langley Research Center. This software system is capable of generating grids on complex configurations, analyzing the grids with a flow solver, and postprocessing the results. TetrUSS is composed of several components, including GridTool, VGRIDns, USM3D, and ViGPLOT. GridTool and VGRIDns are used to generate unstructured tetrahedral grids that can then be analyzed by the USM3D Navier–Stokes flow solver. Although not used during this study, the ViGPLOT flow visualization program can be used to postprocess the flow solutions generated by USM3D.

The grid-generation process is begun using GridTool. In GridTool, a series of points and curves are used to form patches on the surface of the geometry. In addition, sources that control the size and density of the cells in the grid are created in GridTool. VGRIDns [9] then uses these patches and sources to generate an unstructured tetrahedral grid. VGRIDns uses the advancing-layers method to generate unstructured cells in the boundary layer and the advancing-front method to generate cells in the inviscid region of the grid.

USM3D [10] is a three-dimensional, cell-centered, finite-volume Navier–Stokes flow solver for unstructured, tetrahedral meshes. Under the CST portfolio and jointly with the Naval Air Systems Command, USM3D has been enhanced to improve performance and increase capability. USM3D uses Roe's flux-difference splitting technique to compute the inviscid flux quantities across each cell face. The MinMod flux limiter was also implemented within USM3D for this study. The implicit Gauss–Seidel time-stepping scheme was used to advance the solution to a steady-state condition. USM3D is capable of performing both steady-state and time-accurate calculations. Whereas the majority of the calculations for this study were conducted with USM3D in steady-state mode, time-accurate calculations were conducted at a single high-angle-of-attack condition to show the benefits of time-accurate calculations.

The one-equation SA turbulence model [11] and the two-equation Menter's shear stress transport (SST) model [12] are available within USM3D. DES is also available with SA and SST for time-accurate calculations.

IV. Geometry and Grid Descriptions

A. Geometry Description

The geometry evaluated during this computational study was that of the 15%-scale preproduction F/A-18E wind-tunnel model with full nose-down control as shown in Fig. 1. The wing was modeled with 34/4/0 flaps, indicating that the leading-edge flap was deflected 34 deg, the trailing-edge flap was deflected 4 deg, and the aileron was not deflected. The geometry was modeled with both horizontal and vertical tails present. Horizontal-tail deflections of 0 and 20 deg were evaluated. The rudders were toed out 30 deg. The model also included a LEX spoiler, which was deflected 60 deg. A Sidewinder missile and launcher were modeled at the wing tip, and the inlet was modeled as flow through. A dual-sting was also included in the CFD geometry, extending 3.5 fuselage lengths downstream of the aircraft. The sting was modeled as a viscous surface, but the forces and moments on the sting were not included in the total aircraft force and moment calculations. An afterburner nozzle was also included in the geometry.

The 15%-scale wind-tunnel model had an internal cavity in the aft part of the model. This cavity was modeled in the CFD geometry and is shown in Fig. 2. The air entered the open cavity via the inlet duct and exited the cavity through the nozzle. The mounting plate was also included in the geometry. The sting was attached to the mounting plate and extended through the nozzle and downstream of the aircraft.

B. Grid Descriptions

Four different computational grids were used during this project. Three of these grids represented the preproduction F/A-18E with full nose-down control with a horizontal-tail deflection of 20 deg. The fourth grid was of the preproduction F/A-18E with neutral nose-down control with a horizontal-tail deflection of 0 deg. In each of these grids, only half of the aircraft was modeled, and a symmetry-plane boundary condition was implemented. All of the grids generated during this study had viscous tetrahedral cells near the surface and inviscid tetrahedral cells away from the surface. The y-plus value of the first cell above the surface was approximately unity for each of the grids.

1. *Coarse Grids*

Two coarse grids were generated during this project. The first grid had a horizontal-tail deflection of 20 deg, representing the preproduction F/A-18E with full nose-down control. Images of this grid are shown in Figs. 3–5. The second grid had a horizontal-tail deflection of 0 deg. The only geometric difference between these two grids was the deflection of the horizontal tail. Each grid contained 9.9 million cells.

2. *Fine Grid*

A fine grid with 18.0 million cells was generated on the F/A-18E with full nose-down control. This grid and the 9.9-million-cell coarse

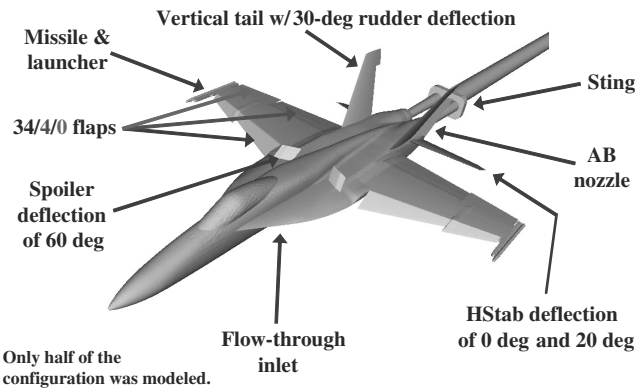

Fig. 1 Computational geometry of the 15%-scale wind-tunnel model of the preproduction F/A-18E Super Hornet considered during this study.

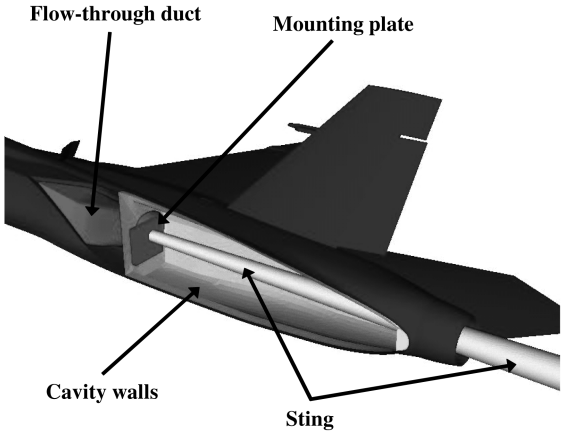

Fig. 2 Internal geometry of the CFD grid of the 15%-scale wind-tunnel model.

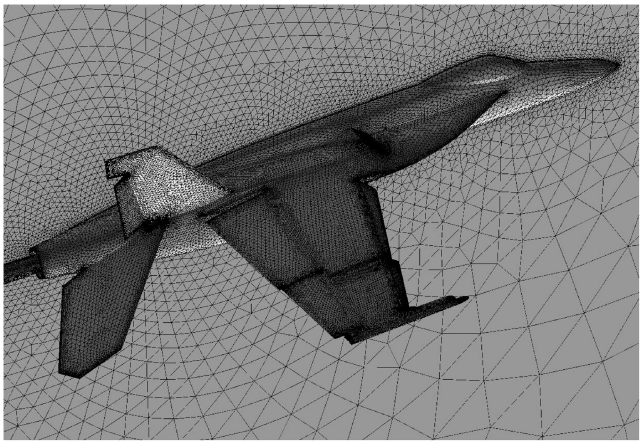

Fig. 3 Side view of the 9.9-million-cell coarse grid with wing flaps deflected to 34/4/0, rudder deflected 30 deg outboard, horizontal tail deflected 20 deg, and the LEX spoiler deflected 60 deg.

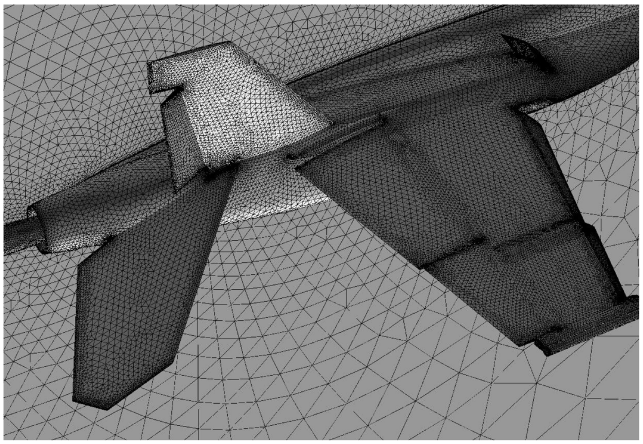

Fig. 4 Surface grid for the wing, tails, and spoiler of the 9.9-million-cell coarse grid.

grid discussed previously were used as part of the initial grid-resolution study.

3. Refined Grid

A refined grid with 19.9 million cells was made for the F/A-18E with full nose-down control. This grid had additional cells above the LEX, wing, and horizontal tail to better resolve the flow in the wake.

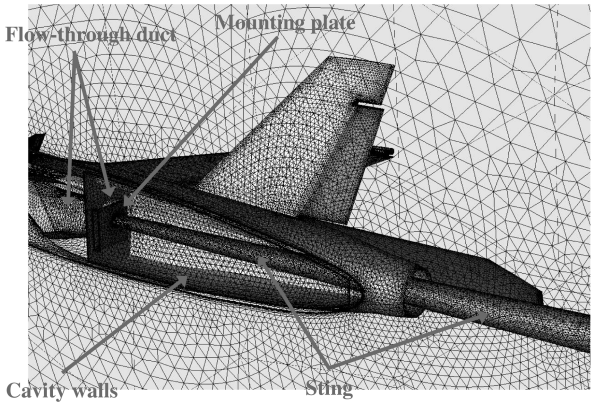

Fig. 5 Surface grid for the sting, mounting plate, and cavity of the 9.9-million-cell coarse grid.

The refined grid was generated by adding sources in GridTool above the LEX, wing, and horizontal tail. A picture of the GridTool sources is shown in Fig. 6.

V. Computer Requirements and Solution Convergence

Both steady-state and time-accurate calculations were conducted during this study. The steady-state calculations presented in this paper were performed on SGI Origin 3800/3900 machines, and the time-accurate calculations were performed on an SGI Altix 4700. These machines were provided by the DOD High Performance Computing Modernization Office (HPCMO). The steady-state cases were run using either 32 or 64 processors, whereas the time-accurate cases were run using 128 processors. Table 1 shows the computer time required for the grid-resolution study and each phase of the longitudinal study. The total CPU time required for this project is less than the sum of the totals in Table 1, because some of the results from the grid-resolution study were used for the longitudinal study. Note that the SGI Altix 4700 is three or four times faster than the SGI Origin 3800/3900 machines. In addition, performance enhancements were made to USM3D between the time when the steady-state calculations were conducted and the time when the time-accurate calculations were conducted, allowing USM3D to run 3.5 times faster. These distinctions make it appear that time-accurate calculations are less expensive than steady-state calculations. In reality, these time-accurate calculations were approximately 10 times more expensive than the equivalent steady-state calculations.

The steady-state solutions were deemed "converged" when the total lift, drag, and pitching-moment coefficients on the viscous surfaces did not change more than 0.0001 in 500 iterations. Whereas most of the solutions using the SA turbulence model achieved this convergence criterion, the solutions using the SST turbulence model failed to achieve this convergence criterion. The convergence characteristics of the cases using SST will be discussed later in this paper.

VI. Initial Grid-Resolution Study

Coarse and fine grids with 9.9 and 18.0 million cells, respectively, were used to perform a grid-refinement study on the preproduction F/A-18E configuration with full nose-down control. The calculations were performed with steady-state assumptions for Mach 0.082 at angles of attack between 5 and 35 deg using the SA turbulence model. The lift and pitching-moment coefficients for these two grids are compared in Fig. 7. From this figure, it can be seen that the lift and pitching-moment coefficients are nearly identical for the two grids. As a result, the 9.9-million-cell grid was used to perform the calculations for angles of attack between 0 and 60 deg. Initially, high-angle-of-attack calculations up to 35 deg angle of attack were to be considered during this project. As a result, the grid-refinement study extended to only 35 deg angle of attack. After the grid-refinement study was completed and the calculations were initiated, however, it

Table 1 Number of solutions and CPU requirements for the grid-resolution and longitudinal studies

Study	Number of solutions	CPU time, hr
Initial grid-resolution study (steady state)	8	137,000
Calculations with $\delta_s = 0$ deg using 9.9 million cells with SA (steady state)	7	90,000
Calculations with $\delta_s = 20$ deg using 9.9 million cells with SA (steady state)	14	173,000
Calculations with $\delta_s = 20$ deg using 19.9 million cells with SA (steady state)	1	32,000
Calculations with $\delta_s = 20$ deg using 9.9 million cells with SST (steady state)	1	20,000
Calculations with $\delta_s = 20$ deg using 19.9 million cells with SST (steady state)	8	332,000
Time-accurate calculations with $\delta_s = 20$ deg using 19.9 million cells (using a different computer and different version of USM3D)	4	102,000

was decided to continue the calculations into the extreme-angle-of-attack regime beyond wing stall.

VII. Longitudinal Stability and Control Predictions

The 9.9-million-cell coarse grids with horizontal-tail deflections of 0 and 20 deg were analyzed in steady-state mode for Mach 0.082 and $Re_c = 1.15 \times 10^6$ for several angles of attack between 0 and 60 deg using the SA turbulence model. These calculations were performed blind without any knowledge of the existing wind-tunnel data. In Figs. 8–12, the lift, drag, pitching-moment, axial-force, and normal-force coefficients for the two configurations are compared with the wind-tunnel data. Vertical axes are not quantified to permit the release of the data; however, relative differences between the CFD results and the wind-tunnel data can be determined.

For angles of attack up to 40 deg, the CFD results compare very well with the wind-tunnel data. CFD accurately predicted the maximum lift coefficient of the configuration, which occurs at $\alpha = 30$ deg for the wind-tunnel data. CFD also accurately predicted the angle of attack and pitching-moment coefficient in which the minimal amount of pitching moment occurs for full nose-down control for recovery from high-angle-of-attack conditions ("pinch point"). The pinch point is shown in the right-hand plot of Fig. 10 at $\alpha = 40$ deg.

In general, the CFD results did not compare well to the wind-tunnel data for angles of attack above $\alpha = 40$ deg. The lift, drag, pitching-moment, and normal-force coefficients show a change in slope at $\alpha = 35$ deg. Below $\alpha = 35$ deg, the burst location of the LEX vortex moves forward as the angle of attack is increased. At $\alpha = 35$ deg, the burst of the LEX vortex reaches the apex of the LEX, causing the slope change that is evident in the plots. The CFD results do not exhibit a slope change at $\alpha = 35$ deg, resulting in a disagreement between the CFD results and the wind-tunnel data at angles of attack above $\alpha = 40$ deg.

The axial-force coefficient predicted by CFD agreed well with the wind-tunnel data over the entire range of angle of attack considered for these calculations.

Using the plots of the pitching-moment coefficient shown in Fig. 10, the pitching-moment increment was calculated to determine the tail effectiveness. The resulting pitching-moment increment for the CFD calculations and the wind-tunnel test are plotted in Fig. 13. Despite the poor correlation of the CFD results at the higher angles of attack for the absolute force and moment coefficients, CFD accurately predicted the increment in pitching-moment coefficient.

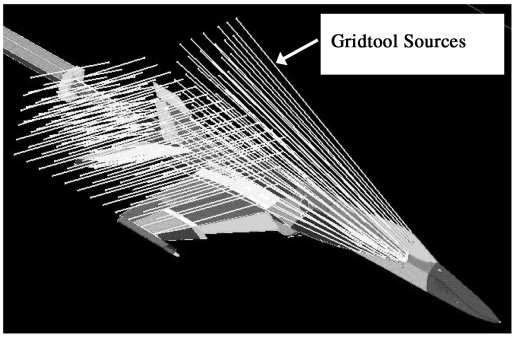

Fig. 6 GridTool sources used to generate the refined 19.9-million-cell grid of the preproduction F/A-18E with full nose-down control.

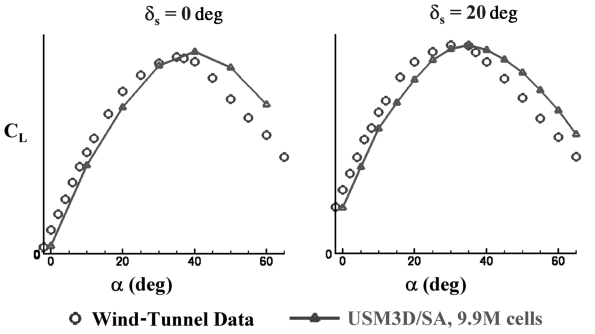

Fig. 8 Lift coefficient variation with angle of attack for the wind-tunnel data and steady-state USM3D at Mach 0.082 and $Re_c = 1.15 \times 10^6$ for tail deflections of 0 and 20 deg.

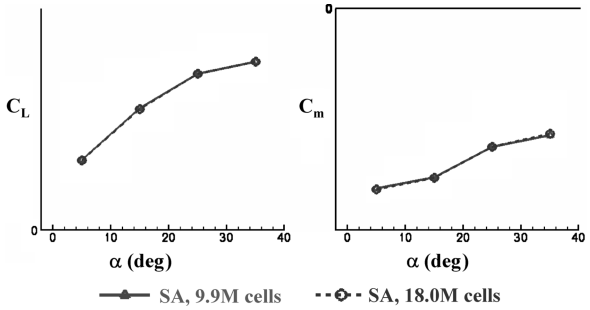

Fig. 7 Comparison of lift and pitching-moment coefficients between 9.9- and 18.0-million-cell grids of the F/A-18E with full nose-down control at Mach 0.082 and $Re_c = 1.15 \times 10^6$ with USM3D in steady-state mode.

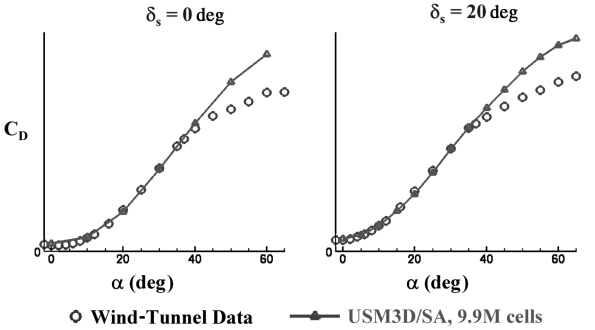

Fig. 9 Drag coefficient variation with angle of attack for the wind-tunnel data and steady-state USM3D at Mach 0.082 and $Re_c = 1.15 \times 10^6$ for tail deflections of 0 and 20 deg.

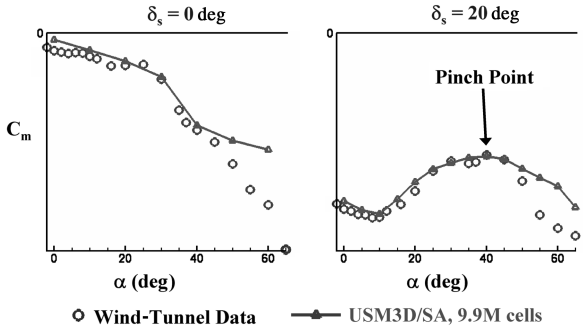

Fig. 10 Pitching-moment coefficient variation with angle of attack for the wind-tunnel data and steady-state USM3D at Mach 0.082 and $Re_c = 1.15 \times 10^6$ for tail deflections of 0 and 20 deg.

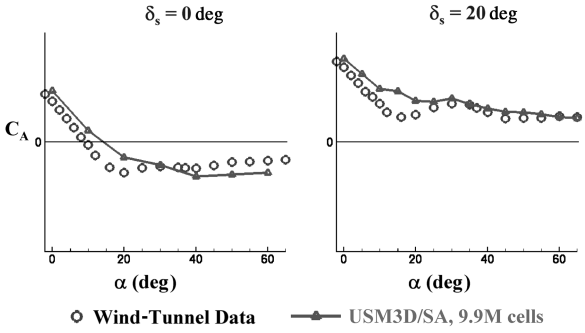

Fig. 11 Axial-force coefficient variation with angle of attack for the wind-tunnel data and steady-state USM3D at Mach 0.082 and $Re_c = 1.15 \times 10^6$ for tail deflections of 0 and 20 deg.

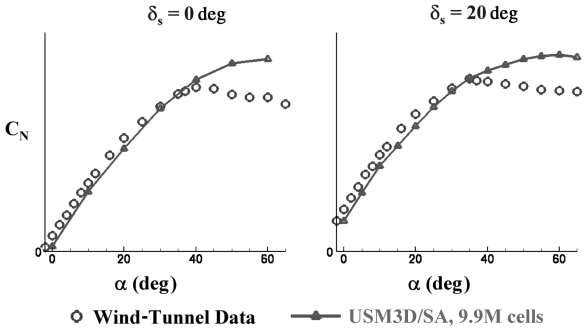

Fig. 12 Normal-force coefficient variation with angle of attack for the wind-tunnel data and steady-state USM3D at Mach 0.082 and $Re_c = 1.15 \times 10^6$ for tail deflections of 0 and 20 deg.

VIII. Impact of Turbulence Model and Grid Density

In an effort to understand the reasons for the poor correlation between CFD and wind-tunnel results at the higher angles of attack, the impact of turbulence model and grid density was investigated. All of the results presented in the preceding section were generated using the SA turbulence model on a grid with 9.9 million cells. In an effort to better resolve the flow in the wake, a refined grid with 19.9 million cells was generated, as previously discussed. This refined grid was used with the SST turbulence model in steady-state mode to determine if a better correlation with the wind-tunnel data could be obtained for angles of attack between 0 and 60 deg. The results for the lift, drag, pitching-moment, axial-force, and normal-force coefficients are presented in Fig. 14. For completeness, the SST turbulence model was used on the 9.9-million-cell grid, and the SA turbulence model was used on the 19.9-million-cell grid at $\alpha = 60$ deg. These results are also included in Fig. 14.

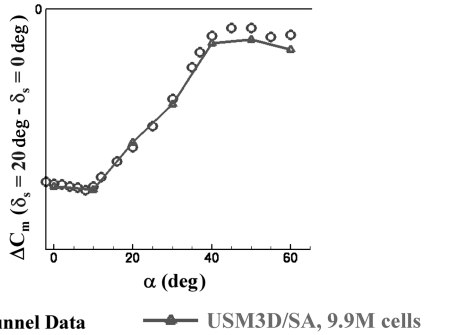

Fig. 13 Variation of pitching-moment increment due to tail deflection with angle of attack for tail deflections of 0 and 20 deg at Mach 0.082 and $Re_c = 1.15 \times 10^6$.

The first major conclusion from Fig. 14 is that the results are not grid dependent at $\alpha = 60$ deg. This is the only angle of attack at which both turbulence models were used with both grids. It is assumed that the results for all angles of attack between 0 and 60 deg are not grid dependent. This conclusion is partially substantiated by the results of the initial grid-resolution study discussed previously and presented in Fig. 7.

In general, the results in Fig. 14 indicate that the use of the SST turbulence model correlates better with the wind-tunnel data at the higher angles of attack. The SST turbulence model also seems to predict the slope change evident in the data at $\alpha = 35$ deg. This improved correlation with SST at the higher angles of attack is likely

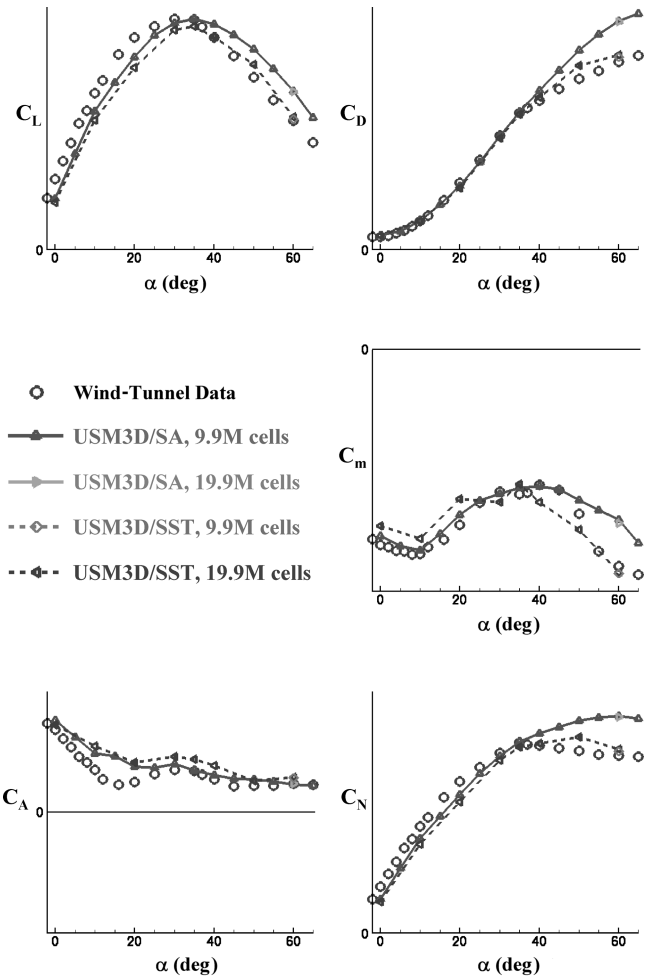

Fig. 14 Variation of lift, drag, pitching-moment, axial-force, and normal-force coefficients with angle of attack for the F/A-18E with a tail deflection of 20 deg at Mach 0.082 and $Re_c = 1.15 \times 10^6$ for wind-tunnel data and steady-state USM3D for two grids and two turbulence models.

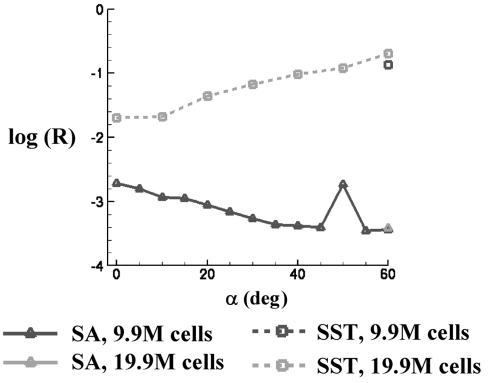

Fig. 15 The L-2 norm of the mean-flow residual as a function of angle of attack for the 9.9- and 19.9-million-cell grids with the SA and SST turbulence models.

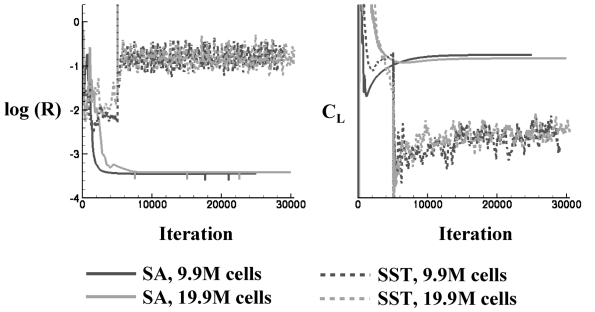

Fig. 16 The L-2 norm of the mean-flow residual and lift coefficient as a function of iteration for the 9.9- and 19.9-million-cell grids with the SA and SST turbulence models at Mach 0.082, $Re_c = 1.15 \times 10^6$ and an angle of attack of 60 deg.

a result of the fact that SST is less dissipative than SA, allowing the vortices to better convect downstream and impact other surfaces of the aircraft. The SA turbulence model correlates better with the data at the lower angles of attack. The difference in the pitching-moment coefficient between SA and SST at the lower angles of attack is clearly evident.

Whereas the correlation between SST and the wind-tunnel data is fairly good, the convergence characteristics of the solutions using the SST model for this application were less than ideal. In Fig. 15, the L-2 norm of the mean-flow residual is plotted as a function of angle of attack for the 9.9- and 19.9-million-cell grids with the SA and SST turbulence models. For all cases, the solutions using the SA turbulence model converged to better than 2.6 orders of magnitude. The solutions using the SST turbulence model, on the other hand, converged to less than 1.8 orders of magnitude. At $\alpha = 60$ deg, the calculation using SST failed to converge to 1 order of magnitude.

The convergence characteristics at $\alpha = 60$ deg for the SA and SST turbulence models are shown in Fig. 16, where the residual and lift coefficient are plotted as a function of iteration number. The solution using the SA turbulence model converges well. The residual flattened out after 10,000 iterations, and the lift flattened out after 15,000 iterations for both the 9.9- and the 19.9-million-cell grids. The residual and lift for the solution using the SST model, on the other hand, are still oscillating after 30,000 iterations.

This author has used USM3D with SST for non-F/A-18 configurations at low-speed, low angle-of-attack conditions. For those calculations, USM3D with SST did converge to more than 3 orders of magnitude. It is possible that the convergence characteristics obtained during this study for SST are specific to the F/A-18 configuration. Further applications of USM3D with SST are necessary to gain a better understanding of its general convergence characteristics.

IX. Time-Accurate Calculations

All of the calculations presented previously were generated with USM3D in steady-state mode. Whereas the original plan for this project was exploratory in nature and did not include any time-accurate calculations, the very nature of unsteady flows at high angle-of-attack conditions immediately raises the issue of using steady-state solutions. Accordingly, time-accurate calculations using USM3D in time-accurate mode were conducted on the 19.9-million-cell grid to assess the impact of unsteady methods at $\alpha = 60$ deg. The SA, SST, DES/SA, and DES/SST turbulence models were evaluated during this study and are compared with the steady-state USM3D calculations in Figs. 17–19, where the lift, drag, and pitching-moment coefficients are presented. These results suggest that running SA in time-accurate mode did not significantly improve the correlation between CFD and the wind-tunnel data. In fact, Fig. 19 indicates that the steady-state SA results correlate better with the data than the time-accurate SA results. The steady-state and time-accurate SA results presented herein suggest that the SA turbulence

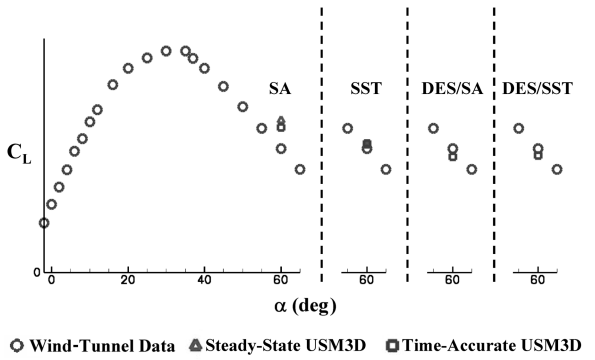

Fig. 17 Variation of lift coefficient with angle of attack for the F/A-18E with a tail deflection of 20 deg at Mach 0.082 and $Re_c = 1.15 \times 10^6$ for wind-tunnel data and USM3D in steady-state and time-accurate mode for several different turbulence models on the 19.9-million-cell grid.

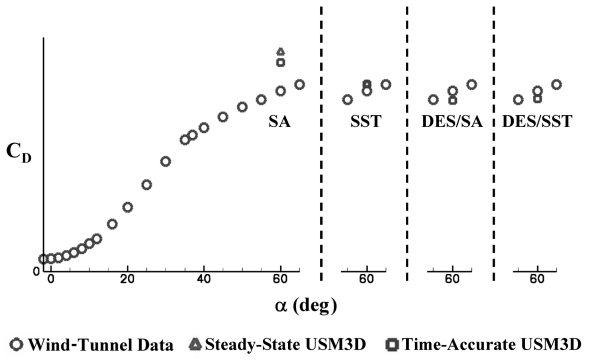

Fig. 18 Variation of drag coefficient with angle of attack for the F/A-18E with a tail deflection of 20 deg at Mach 0.082 and $Re_c = 1.15 \times 10^6$ for wind-tunnel data and USM3D in steady-state and time-accurate mode for several different turbulence models on the 19.9-million-cell grid.

model is not accurate for low-speed, high angle-of-attack calculations on the F/A-18.

Furthermore, the results suggest that running SST in time-accurate mode does not provide a better correlation between CFD and the wind-tunnel data at $\alpha = 60$ deg. In Fig. 19, it can be seen that the pitching-moment coefficient from the steady-state and time-accurate SST calculations deviated about the same amount from the wind-tunnel data. Whereas the time-accurate SST calculations did not improve the correlation at $\alpha = 60$ deg, it is possible that time-accurate calculations could improve the correlations at $\alpha = 40$ and 50 deg, where differences between steady-state SST and the wind-tunnel data can be noted in Fig. 14.

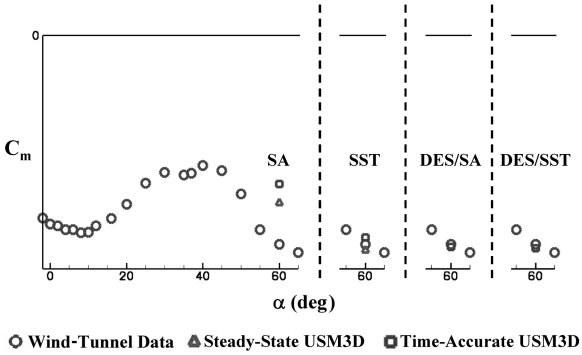

Fig. 19 Variation of pitching-moment coefficient with angle of attack for the F/A-18E with a tail deflection of 20 deg at Mach 0.082 and $Re_c = 1.15 \times 10^6$ for wind-tunnel data and USM3D in steady-state and time-accurate mode for several different turbulence models on the 19.9-million-cell grid.

Figures 17–19 also indicate that, when DES is combined with either the SA or SST models, a good correlation with the wind-tunnel data is obtained. This is not unexpected, given the large amount of flow separation that would be expected at low-speed, high angle of attacks.

In regard to the convergence issues with SST in steady-state mode, it is important to note here that SST in time-accurate mode converged at least 2 orders of magnitude in the L-2 norm of the mean-flow residual. Recall from Fig. 15 that SST in steady-state mode did not converge to this level.

X. Conclusions

Computational fluid dynamics has been used to predict the longitudinal stability and control characteristics of the preproduction F/A-18E with neutral and full nose-down control at low-speed, high-angle-of-attack conditions. Calculations were performed for Mach 0.082 for angles of attack between 0 and 60 deg with the USM3D flow solver. The results of this study indicate that the Spalart–Allmaras turbulence model with steady-state flow assumptions accurately predicted the forces and moments for angles of attack below 40 deg. Above 40 deg, however, the Spalart–Allmaras turbulence model could not accurately predict forces and moments. The Spalart–Allmaras turbulence model, however, did calculate the pitching-moment increment accurately for angles of attack between 0 and 60 deg. Spalart–Allmaras accurately predicted the angle of attack for minimum nose-down control (pinch point) as well as the magnitude of the pinch point of the aircraft. Menter's shear stress transport model was used in steady-state mode to predict the forces and moments at high angles-of-attack with some success. The results at high angles of attack with the Spalart–Allmaras and shear stress transport were not improved with time-accurate calculations. The time-accurate results do indicate, though, that detached-eddy simulation could improve the accuracy at the higher angles of attack.

This study was the second phase of exploratory calculations being performed as part of the portfolio. The first phase involved longitudinal and lateral/directional stability and control predictions on the preproduction F/A-18E at transonic speeds. Based on the combined results of these two CFD studies, considerable optimism exists for the application of computational methods for future high-performance aircraft. Such applications would allow the designer to augment his or her existing toolbox to extrapolate experimental predictions to higher values of Reynolds number, provide flow diagnostic capability for stability and control problems, and provide analysis capabilities in which wind-tunnel techniques are not available. Additional requirements for stability and control analysis, such as aircraft dynamic-motion effects on aerodynamics, might be particularly fruitful areas of research in the near future. Additional calibrations of computational fluid dynamics methods for other airplane configurations will also be required to convince the engineering community that computational fluid dynamics is a viable predictive tool for critical high-angle-of-attack conditions. Finally, more sophisticated experimental data in the form of surface pressures and off-surface flow visualization and characterization would be helpful in calibrating codes. A collaborative experimental/computational study is highly recommended for future thrusts in this area.

Acknowledgments

The author would like to gratefully acknowledge the funding that was granted for this study by the HPCMO through the CST portfolio. In addition, the author would like to thank David Findlay and James Chung for their guidance and insight. Also, the author would like to thank the HPCMO for the many hours of computer time that was necessary to complete this computational study. Finally, the author acknowledges the advice and guidance of the following individuals: Steve Hynes and Alex Kokolios of the Naval Air Systems Command; Robert Hall, Neal Frink, and Mike Fremaux of NASA Langley Research Center; Joseph Chambers, retired NASA Langley Research Center consultant; and Mohagna Pandya of Analytical Services and Materials. The author would also like to thank Edward Dickes of Bihrle Applied Research for providing the wind-tunnel test data (with permission of the Navy and the Boeing Company) and information about the test that was used to validate the CFD calculations.

References

[1] Chambers, J. R., and Hall, R. M., "Historical Review of Uncommanded Lateral-Directional Motions at Transonic Conditions," *Journal of Aircraft*, Vol. 41, No. 3, 2004, pp. 436–447. doi:10.2514/1.4470

[2] Cummings, R. M., Forsythe, J. R., Morton, S. A., and Squires, K. D., "Computational Challenges in High Angle of Attack Flow Prediction," *Progress in Aerospace Sciences*, Vol. 39, No. 5, July 2003, 369–384.

[3] Spalart, P. R., "Young-Person's Guide to Detached-Eddy Simulation Grids," NASA CR 2001-211032, 2001.

[4] Forsythe, J. R., Squires, K. D., Wurtzler, K. E., and Spalart, P. R., "Detached-Eddy Simulation of the F-15E at High Alpha," *Journal of Aircraft*, Vol. 41, No. 2, 2004, pp. 193–200. doi:10.2514/1.2111

[5] Forsythe, J. R., Squires, K. D., Wurtzler, K. E., and Spalart, P. R., "Prescribed Spin of the F-15E using Detached-Eddy Simulation," AIAA Paper 2003-839, 2003.

[6] Green, B. E., and Chung, J. J., "Transonic Computational Fluid Dynamics Calculations on Preproduction F/A-18E for Stability and Control," *Journal of Aircraft*, Vol. 44, No. 2, 2007, pp. 420–426. doi:10.2514/1.22846

[7] Britcher, C. P., and Landman, D., "From the 30 by 60 to the Langley Full Scale Tunnel," AIAA Paper 98-145, Jan 1998.

[8] Frink, N. T., Pirzadeh, S., Parikh, P., Pandya, M. J., and Bhat, M. K., "The NASA Tetrahedral Unstructured Software System (TetrUSS)," *The Aeronautical Journal*, Vol. 104, No. 1040, 2000, pp. 491–499.

[9] Pirzadeh, S., "Three-Dimensional Unstructured Viscous Grids by the Advancing Layers Method," *AIAA Journal*, Vol. 34, No. 1, 1996, pp. 43–49.

[10] Frink, N. T., "Tetrahedral Unstructured Navier–Stokes Method for Turbulent Flows," *AIAA Journal*, Vol. 36, No. 11, 1998, pp. 1975–1982.

[11] Spalart, P. R., and Allmaras, S. R., "A One-Equation Turbulence Model for Aerodynamic Flows," AIAA Paper 97-0644, Jan. 1997.

[12] Menter, F. R., "Zonal Two Equation k–ω Turbulence Models for Aerodynamic Flows," AIAA Paper 93-2906, July 1993.